International Journal of Solids and Structures 48 (2011) 1070–1081

Contents lists available at ScienceDirect

International Journal of Solids and Structures

journal homepage: www.elsevier.com/locate/ijsolstr

Simulation and experimental validation of mixed mode delamination in multidirectional CF/PEEK laminates under fatigue loading

P. Naghipour [a,b,*], M. Bartsch [a], H. Voggenreiter [a,b]

[a] Institute of Materials Research, German Aerospace Center (DLR), Linder Hoehe, 51147 Cologne, Germany
[b] Institute of Aircraft Design (IFB), University of Stuttgart, Pfaffenwaldring 31, 70569 Stuttgart, Germany

ARTICLE INFO

Article history:
Received 23 March 2010
Received in revised form 15 October 2010
Available online 28 December 2010

Keywords:
Composite materials
Delamination
Finite elements
Fiber reinforced
Fracture
Fatigue

ABSTRACT

Cyclic mixed mode delamination in multidirectional composite laminates subjected to high cycle fatigue loading has been investigated by numerical simulations and cyclic mixed mode bending experiments. The numerical model includes lamina and interface elements. The description of the delamination crack growth rate is based on the cyclic degradation of bilinear interface elements linking the evolution of the damage variable with the delamination crack growth rate. The constitutive cyclic damage model is calibrated by means of mixed mode fatigue experiments and reproduces the experimental results successfully and with minor error. It is concluded that only with implementing a cyclic damage variable in the cohesive interface element the experimentally observed crack growth and stiffness degradation can be captured properly. Scanning electron microscopy of fracture surfaces after cyclic loading revealed that abrasion of crack bridging surface roughness is the main microscopical cause of weakening and degradation of the interface.

1. Introduction

The need for light weight structural materials with good resistance to fatigue has led designers of aircrafts to increasingly employ CFRP structures, when cyclic loading is of primary concern. The growth of the damage under subsequent fatigue loads may lead to final catastrophic failure of the component. Thus, predicting the extent of fatigue damage growth through development of an accurate fatigue damage model is essential to the continued employment of CFRP structures into even more demanding aerospace applications. One of the most common types of damage observed in CFRP composites subjected to cyclic loading is delamination. Typically, delamination failures initiate and propagate under mixed mode effect of normal and shear stresses. Therefore, in order to have a thorough understanding of the cyclic mixed mode delamination mechanism in CFRP structures, development of a reliable and predictive analysis tool has been one of the issues studied extensively by the aerospace industry.

There are diverse approaches to study the fatigue delamination phenomenon in composite materials. Among the most representative experimental approaches for description of the fatigue behaviour are fatigue life models, which predict the number of cycles corresponding to fatigue failure under fixed loading conditions (Ex. mixed mode delamination here) using an experimentally determined failure criterion (Andersons, 1994; Reifsnider, 1991; Suresh, 1991 or Talreja, 1999). The second approach can be classified as fatigue related fracture models, which basically study rate of crack growth under cyclic loading (Ex. mixed mode cyclic delamination). Fracture mechanics models relate the variation of the energy for formation of two new crack surfaces with the crack growth (Dowling and Begley, 1976; Ewalds, 1984; McDowell, 1997; Paris et al., 1961; Paris and Erdogan, 1963 or Rice, 1980). The fatigue crack propagation rate is denoted by dA/dN, where A is the crack area, or da/dN, where a is the characteristic crack length. The correlation of the fatigue crack growth rate with the amplitude of the energy release rate, ΔG (or stress intensity factor, ΔK) is commonly represented in a log–log diagram known as Paris plot (Paris et al., 1961; Paris and Erdogan, 1963). The Paris law, describing crack growth versus energy release rate is widely used and accepted among other empirical or semi-empirical crack growth laws. According to this law, the crack growth rate is related to the energy release rate range by a power law that can be expressed as

$$\frac{\partial A}{\partial N} = C\left(\frac{\Delta G}{G_c}\right)^m. \tag{1}$$

The parameters C and m (Paris plot parameters) must be determined experimentally. The energy release rate range, ΔG, depends on the loading conditions, and G_c is the critical energy release rate of the material. Finally, the third approach and meanwhile one of

* Corresponding author at: Institute of Materials Research, German Aerospace Center (DLR), Linder Hoehe, 51147 Cologne, Germany. Tel.: +49 2203 6013509; fax: +49 2203 696480.
E-mail address: parya.naghipour@dlr.de (P. Naghipour).

0020-7683/$ - see front matter © 2010 Elsevier Ltd. All rights reserved.
doi:10.1016/j.ijsolstr.2010.12.012

the most successful techniques used to model cyclic as well as quasi-static delamination in composites relies on the modelling of cohesive zones (Alfano and Crisfield, 2001; Allix and Blanchard, 2006; Barenblatt, 1962; Dugdale, 1960; Harper and Hallett, 2008; Maiti and Geubelle, 2005; Munoz et al., 2006; Naghipour et al., 2009a; Nguyen et al., 2001; Peerlings et al., 2000; Roe and Siegmund, 2003; Serebrinsky and Ortiz, 2005; Turon et al., 2007a; Turon et al., 2007b or Yang et al., 2001). This approach has been also used in this work for the modelling of mixed mode inter-laminar delamination under cyclic and quasi-static loadings.

The cohesive zone technique, first suggested by Dugdale and Barenblatt (Barenblatt, 1962; Dugdale, 1960), is based on using interface element technique for prediction of crack initiation and propagation (Alfano and Crisfield, 2001; Allix and Blanchard, 2006; Harper and Hallett, 2008 or Turon et al., 2007a). As subjected to cyclic loading, the constitutive law of the interface element must be reformulated to account for subcritical damage accumulation and stiffness degradation within subsequent unloading–reloading steps (Maiti and Geubelle, 2005; Munoz et al., 2006; Nguyen et al., 2001; Peerlings et al., 2000; Roe and Siegmund, 2003; Serebrinsky and Ortiz, 2005; Turon et al., 2007b or Yang et al., 2001). Though there is a wealth of experimental results on fatigue crack propagation in quasi-brittle materials, like fibre reinforced composites, very few attempts have been undertaken to numerically model fatigue crack propagation by cohesive technique. Yang et al. (2001) modelled fatigue crack growth in quasi-brittle materials using a cohesive zone model incorporating an irreversible damage, which is assumed to accumulate not only along the damage locus but also during any unloading–reloading path. This idea makes it possible to predict the sub-critical crack growth due to cyclic loading, which occurs before reaching the damage locus under quasi-static conditions. Therefore, the fatigue damage behaviour of a material may be studied under any arbitrary loading condition provided that the properties of the cohesive zone are specified correctly. They have also proposed a cohesive law in a general polynomial form, representing different stiffness (k) expressions for unloading and reloading paths. The predicted reduction of stiffness due to each cycle is specified in the suggested polynomial logarithmic cohesive law by Yang et al. (2001)). Later, Roe and Siegmund (2003) addressed the cyclic degradation by substituting the initial cohesive strengths with the current degraded cohesive strengths during successive loading steps. In other words, during each unloading and reloading cycle, the mentioned tractions or strengths are degraded by a scalar damage factor $(1 - D_c)$, where $D_c(0 < D_c < 1)$ stands for the damage parameter. The evolution equation for D_c as a function of effective cohesive strengths has been explicitly specified in their work (Roe and Siegmund, 2003). Maiti and Geubelle (2005) developed a model, which relies on the combination of a bi-linear cohesive failure law used for fracture simulations under monotonic loading and an evolution law relating the cyclic degradation of the cohesive stiffness with the rate of crack opening displacement and the number of cycles since the onset of damage evolution. The fatigue component of the cohesive model involves two parameters that can be readily calibrated based on the classical log–log Paris relation between the crack advance per cycle and the range of applied stress intensity factor. According to Maiti and Geubelle (2005), under cyclic loading the evolution law of the instantaneous cohesive stiffness can be expressed with an exponential decay function. The cohesive strength decays exponentially and the rate of decay is controlled by a power law relation as a function of number of cycles (N) (Maiti and Geubelle, 2005). Yet, another similar approach presented by Serebrinsky and Ortiz (2005), Nguyen et al. (2001) states that for fatigue applications, the material stiffness must be degraded in the reloading phase of each cycle. The cohesive element/zone is cycled at amplitudes smaller than the cohesive envelope. Therefore, a simple phenomenological model, which embodies these assumptions, is obtained by assuming different incremental stiffnesses K^+ and K^- depending on whether the cohesive interface opens (is reloaded) or closes (is unloaded). The evolution law for the mentioned reloading stiffness is assumed to be a function of crack opening displacement in each unloading–reloading cycle (Serebrinsky and Ortiz, 2005). In Munoz et al. (2006) it is stated that an alternative approach for the simulation of fatigue driven delamination growth is to incorporate fatigue degradation into the interface element technique for modeling crack propagation. The fatigue damage evolution law of the interface model given by Munoz et al. (2006) is adapted form Peerling's law (Peerlings et al., 2000) and rewritten for the mixed mode delamination. Under single mode delamination it reduces to the well-known Peerling's law (Peerlings et al., 2000), which assigns an exponential growth for the cyclic damage parameter as a function of the number of cycles and opening displacements. Similar to previously mentioned works, Turon et al. (2007b) also proposed a damage model for the simulation of cyclic delamination growth under high cycle fatigue. The fatigue damage evolution law is a cohesive law that links fracture and damage mechanics to establish the evolution of the damage variable in terms of the crack growth rate da/dN. The model relates damage accumulation to the number of load cycles while taking into account the loading conditions (load ratio, energy release rate, and fracture mode mixity).

The present paper focuses on simulation of fatigue driven mixed mode delamination in multidirectional (MD) CFRP laminates following experimental and numerical approaches. Very few studies on single or mixed mode fatigue delamination have been reported in literature, but no attempts have been undertaken to numerically model the fatigue delamination in multidirectional CFRPs with varying fibre orientations at the delamination interface. Cyclic mixed mode delamination of multidirectional CFRPs is a complicated task, since in an interface with dissimilar fibre orientations in-ply damage states might occur together with delamination and interact with each other evoking the final fracture. The possibility of interacting intra– and inter-laminar damages must also be counted for in the numerical model in order to have a reliable cyclic mixed mode delamination simulation. Therefore, the first element of novelty in this work is development of a precise and predictive numerical tool able to successfully estimate the successive loss of load bearing capacity, and predict occurring damage modes in multidirectional CFRPs, subjected to cyclic mixed mode delamination. The predictive capability of the numerical model depends strongly on correct identification of the model parameters for interfaces with dissimilar ply orientations (multidirectional interfaces). Meanwhile, the model parameters for mixed mode delaminations vary significantly in multidirectional interfaces susceptible of varying fibre orientations and stacking sequences (Naghipour et al., 2009a). Therefore, cyclic Mixed Mode Bending (MMB) experiments must be specifically conducted on multidirectional specimens (with multidirectional interfaces) to accurately identify model parameters, and to obtain output data for validation of the numerical model. Comprehensive combination of numerical and experimental analysis tools, mainly emphasizing the effect of multidirectional interfaces on mixed mode fatigue delamination of CFRP laminates, has not been addressed in literature and is the second point of novelty in this work. For modelling the mixed mode delamination crack growth under cyclic loading, the following numerical approach incorporates the interface formulation suggested by Turon et al. (2007b), further elaborated by improvements in the cohesive law. The major improvement is modifying the cohesive zone area definition used by Turon et al. (2007b). This definition was developed for pure Mode I loading and the model tends to be less accurate when subjected to mixed mode loading with higher mode II domination. In order to improve the function-

ality and accuracy of the model, in this work the estimation of the cohesive zone area is further improved for a mixed mode load case utilizing the earlier work of Harper and Hallett (2008). Enhancing the order of integration in the implemented user element routine of cohesive elements is the other improvement. Superior accuracy of using higher order integration schemes especially in the case of material or geometrical non-linearity is mentioned by various authors in literature (Alfano and Crisfield, 2001; Bathe, 2001; Szabó and Babuška, 1991). Since the cohesive law is highly non-linear the 3×3 Newton–Cotes integration provides much more accurate and reliable results than lower scheme integrations and therefore has been adopted in this work. The fatigue damage law, together with the above-mentioned improvements, is added to the corresponding constitutive equations in Naghipour et al. (2009a) and implemented as an interface element routine in ABAQUS. The functionality of the numerical model is then validated by predicting the interacting damage states and, by reproducing load reduction in successive cycles of the conducted cyclic MMB experiments.

In Section 2, constitutive equations of the interface element previously implemented in Naghipour et al. (2009a) and the cyclic damage law added to this interface User Element, are explained concisely. In Section 3, production of the multidirectional CFRP specimen, cyclic MMB testing procedure and data reduction methods used, are described. Construction of the numerical model and characterization of input parameters are described in Section 4. Next, in Section 5, numerical simulations of the conducted cyclic mixed-mode delamination experiments are presented to demonstrate the validity of the constitutive fatigue damage model. Discussions on some SEM investigations of exemplary fracture surfaces are also given in this section. Finally, a brief summary and conclusions are presented in Section 6.

2. Interface element and cyclic damage law

2.1. Constitutive formulation of the interface element

The cohesive zone approach adopted in this work and in previous work of the authors (Naghipour et al., 2009a) makes use of interface finite elements incorporating a cohesive mixed-mode damage model. The detailed formulation of the interface element is given in (Naghipour et al., 2009a) and will only be shortly reviewed here. The zero thickness 8-node cohesive element, implemented as a user element (UEL) in ABAQUS (2006), is shown schematically in Fig. 1. Lower face of the interface is represented by nodes 1–4, and the upper surface includes nodes 5–8, which coincide geometrically with nodes 1–4. The global (x,y,z) and local (ξ,η,z) coordinates of the three-dimensional interface element are related by the standard iso-parametric mapping and each node has three degrees of freedom, u, v, and w, in x, y, z directions respectively. Accordingly, the vector of relative displacements between each pair of the corresponding upper and lower nodes is defined as:

$$\begin{bmatrix} \delta_n \\ \delta_s \\ \delta_t \end{bmatrix} = \begin{bmatrix} u_n \\ u_s \\ u_t \end{bmatrix}_{TOP} - \begin{bmatrix} u_n \\ u_s \\ u_t \end{bmatrix}_{BOTTOM}. \tag{2}$$

In Eq. (2), n indicates the normal component and s and t indicate the two shear directions (Fig. 1).

The relationship between the vector of tractions ($\boldsymbol{\tau}$) and relative displacements ($\boldsymbol{\delta}$) in the interface element, shown in Fig. 2, can be written as

$$\tau = \mathbf{D}\boldsymbol{\delta}. \tag{3}$$

In Eq. (3), $\mathbf{D}$ is the interfacial constitutive secant tensor with the isotropic damage parameter, d, given by:

$$\mathbf{D} = \begin{pmatrix} (1-d)K + dKH(-\delta_n) & 0 & 0 \\ 0 & (1-d)K & 0 \\ 0 & 0 & (1-d)K \end{pmatrix}. \tag{4}$$

Due to the highly non-linear cohesive law, 3 integration points are specified in both ξ and η directions and a 3×3 Newton–Cotes integration scheme is used to calculate the damage parameter, d, constitutive tensor, $\boldsymbol{D}$, and relative tractions, $\boldsymbol{\tau}$, in the integration points at each loading increment. Although a 2×2 Newton–Cotes integration scheme (used in Turon et al., 2007b) might accelerate the calculation, it is doubtful to be used with the highly non-linear cohesive law of the element (Alfano and Crisfield, 2001). In Eq. (4), K stands for the initial stiffness of the interface element before any initiation of damage (penalty stiffness). H stands for the Heaviside function ($H(x) = 1$ if $x > 0$), which panelizes compressive direct strains in order to avoid the interpenetration of the interface surfaces. Meanwhile, it also shows that damage, expressed by variable d, does not affect compression stiffness (when $\delta_n < 0$). For the calculation of the extent of damage the scalar-valued damage parameter, d, is introduced. The damage variable, d, is defined as a function of maximum mixed-mode relative displacement in the previous history, δ_m^{max}, initial displacement at delamination onset, δ_m^0, and final separation displacement, δ_m^f (Eq. (5a), Fig. 2).

$$d = \frac{\delta_m^f(\delta_m^{\max} - \delta_m^0)}{\delta_m^{\max}(\delta_m^f - \delta_m^0)}. \tag{5a}$$

The only state variable used to track the damage at the interface is $\delta_m^{max} \cdot \delta_m^0$ is calculated based on the quadratic interfacial traction interaction criterion as a function of mode mixity, m, and single mode normal and shear displacements at delamination onset, δ_n^0 and δ_{shear}^0 respectively (Eq. (5b)).

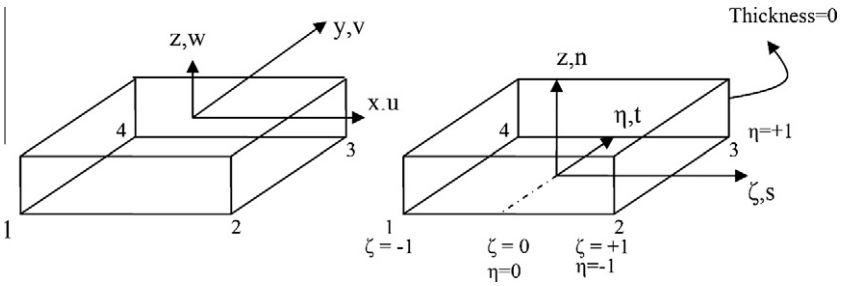

Fig. 1. Interface element with (left) global system and (right) local system (For better visualisation of the zero thickness a virtual thickness is sketched.)

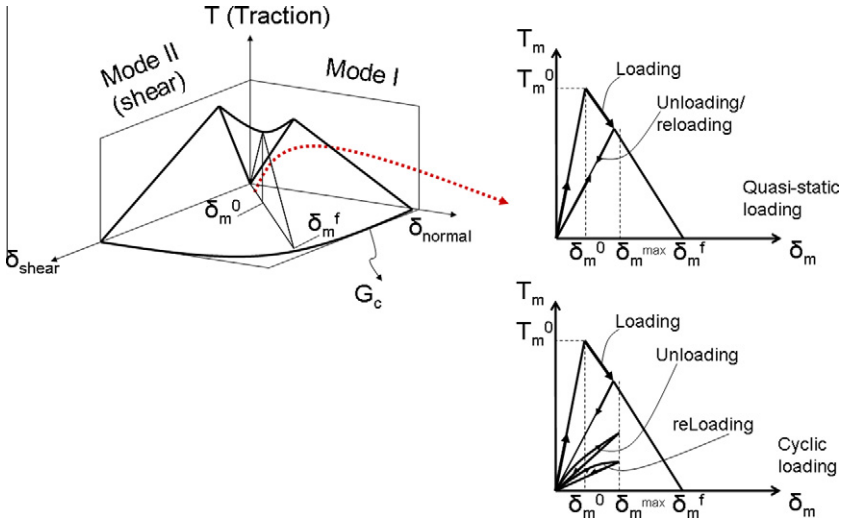

Fig. 2. Cohesive law for mixed mode delamination with linear softening.

$$\delta_m^0 = \left\{ \begin{array}{ll} \delta_n^0 \delta_{shear}^0 \sqrt{\frac{1+m^2}{\left(\delta_{shear}^0\right)^2 + m^2\left(\delta_n^0\right)^2}} & \delta_n > 0 \\ \delta_{shear}^0 & \delta_n < 0 \end{array} \right\} \quad \delta_n^0 = \frac{\tau_n^0}{K},$$

$$\delta_{shear}^0 = \frac{\tau_{shear}^0}{K} \quad m = \frac{\delta_{shear}}{\delta_n}. \tag{5b}$$

Corresponding normal and shear tractions are $\tau_n$and τ_{shear}, related elastically with displacements up to delamination onset (Eq. (5b)). Final separation point, δ_m^f, is derived using an energy based propagation criterion introduced by Benzeggagh and Kenane (B–K) (1996) and corresponds physically to the totally damaged state of the interface element. G_{IC} and G_{IIC} and η appearing in the B–K criterion (Eq. (5c)) stand for mode I, mode II critical strain energy release rates, and the parameter defining the failure locus under mixed mode loading respectively. These parameters have to be determined by mixed mode experiments (Benzeggagh and Kenane, 1996).

$$G_c = G_{IC} + (G_{IIC} - G_{IC})\left(\frac{m^2}{1+m^2}\right)^{\eta} \text{ B-K propagation criteria.} \tag{5c}$$

The damage parameter governs the softening behaviour of the interface and it increases from 0 (no damage) to 1 (complete separation) for monotonous load progression. Mentioned variables are shown schematically in Fig. 2. It must be noted that mode mixity, m, and thus δ_m^f are calculated at each load increment in the written user element code, as under fatigue loading it is quite possible that the mode ratio will change during the life of the interface element.

$$\delta_m^f = \left\{ \begin{array}{cc} \frac{2}{K\delta_m^0}\left[G_{IC} + (G_{IIC} - G_{IC})\left(\frac{m^2}{1+m^2}\right)^{\eta}\right] & (\delta_n > 0) \\ \delta_{shear}^f = \frac{2G_{IIC}}{\tau_s^0} & (\delta_n < 0). \end{array} \right\} \tag{5d}$$

2.2. Damage evolution due to fatigue

A general loading history results in a state of total damage defined as the sum of the damage created by the quasi-static loads and the damage created by the cyclic loads:

$$\frac{\partial d}{\partial t} = \dot{d} = \dot{d}_{quasi-static} + \dot{d}_{cyclic}. \tag{6}$$

The first term in the right hand side of Eq. (6) is obtained from the equations presented in the previous section. In order to define the second term to account for cyclic loading, the approach proposed by Turon et al. (2007b) is further modified by redefinition of the cohesive zone area and is implemented as a user-written element in ABAQUS (2006) by adding the cyclic damage degradation model to the constitutive behavior of the mentioned bi-linear cohesive element. According to Turon et al. (2007b), evolution of the damage parameter with subsequent cycles can be written as:

$$d_{cyclic} = \frac{\partial d}{\partial N} = \frac{\partial d}{\partial A_d}\frac{\partial A_d}{\partial N}. \tag{7}$$

It is worth mentioning that in order to pass from the time derivatives of Eq. (6) to the derivatives with respect to N as in Eq. (7) one has to consider N as a real, time-like variable rather than an integer. The first term in Eq. (7), $\partial d/\partial A_d$, is obtained using the formulation, which relates the damage parameter, d, to the damaged area A_d, in the cohesive section and can be calculated as summarized in Turon et al. (2007b),

$$\frac{\partial d}{\partial A_d} = \frac{1}{A_e}\frac{\left[\delta_m^f(1-d) + d\delta_m^0\right]^2}{\delta_m^0 \delta_m^f}. \tag{8}$$

A_e in Eq. (8) represents the area of a cohesive element. The second term, $\partial A_d/\partial N$, represents the mean value of the damaged area growth rate per element per cycle, $(\partial A_d^e/\partial N)$, in the cohesive zone. The width of the delamination front (numerical damaged area) is assumed to be constant. Therefore the growth of the damage area correlates directly with the growth of the crack length. According to Turon et al. (2007b) the crack growth rate $(\partial A/\partial N)$ can be assumed to be equal to the sum of the damaged area growth rates of all damaged elements ahead of the crack tip as in Eq. (9),

$$\frac{\partial A}{\partial N} = \sum_{e \in A_{cz}} \frac{\partial A_d^e}{\partial N} = \frac{A_{CZ}}{A^e}\frac{\partial A_d}{\partial N},$$
$$\frac{A_{CZ}}{A^e} = \text{number of cohesive elements in the cohesive zone.} \tag{9}$$

The area of the cohesive element can be varied by changing the element length or in other words by changing the mesh size in the cohesive zone. The previous paper of the authors (Naghipour et al., 2009a) shows the sensitivity of the model to cohesive element length. According to our previous work (Naghipour et al., 2009a), comparisons with experimentally obtained results indicate that as long as the interface element size is taken less than 1 mm, a better solution convergence can be achieved for the case of mixed mode

loading. Therefore, here in this paper the cohesive element length is taken as 0.6 mm in all the simulations.

Rearranging the equation above gives the mean surface damage growth rate,

$$\frac{\partial A_d}{\partial N} = \frac{A^e}{A_{cz}} \frac{\partial A}{\partial N}. \tag{10}$$

In order to define the crack growth rate under fatigue loading, $\partial A/\partial N$, the Paris law given in Eq. (1) is embedded in Eq. (10). The growth rate defined by the Paris law represents crack propagation in region II of the typical pattern of the crack growth rate (Fig. 3). When the maximum energy release rate is smaller than the fatigue threshold G_{th} no crack growth is observed. In region III, as the energy release rate approaches the fracture toughness value, a sudden increase is observed in the crack growth rate, and quasi-static fracture controls the crack growth rate in region III instead of fatigue propagation.

Accordingly, rewriting Eq. (7) using Eqs. (8) and (10) gives:

$$\frac{\partial A}{\partial N} = C\left(\frac{\Delta G}{G_c}\right)^m \quad G_{th} < G_{max} < G_c, \tag{11a}$$

$$\frac{\partial d}{\partial N} = \left\{ \begin{array}{cc} \frac{1}{A_{cz}} \frac{(\delta_m^f(1-d)+d\delta_m^0)^2}{\delta_m^f \delta_m^0} C\left(\frac{\Delta G}{G_c}\right)^m & G_{th} < G_{max} < G_c \\ 0 & 0 \end{array} \right\}, \tag{11b}$$

C, m, and G_{th} are Paris plot parameters that are obtained by plotting $\partial A/\partial N$ versus cyclic variation of the energy release rate, ΔG, on log–log scale. G_c is the total mixed mode fracture toughness under a specific mode ratio. In contrast to the work of Turon et al. (2007b) required Paris parameters were calculated directly using the experimental outputs of this work. As mentioned by Blanco et al. (2004) there are several expressions where the cyclic crack propagation rates are expressed by relative contributions of mode I and mode II parameters. However, it has not yet been proved that either of these expressions or the one used in Turon et al. provides the best fit for all types of composite materials. Therefore, the parameters are extracted directly form the related MMB experiments in this work. The maximum energy release rate G_{max} and cyclic variation in the energy release rate ΔG can be computed by the constitutive law of the cohesive zone model using the symmetry of triangles in Fig. 2 as:

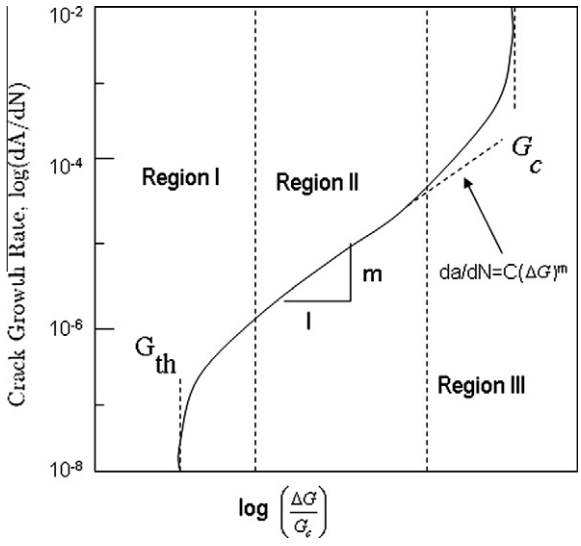

Fig. 3. Schematic of Paris plot describing the crack growth pattern.

$$G_{\max} = \frac{\tau_m^0(\delta_m^f)}{2} - \left(\frac{\delta_m^f - \delta_m^{\max}}{\delta_m^f - \delta_m^0}\right)^2 \frac{\tau_m^0(\delta_m^f - \delta_m^0)}{2},$$
$$G_{\max} = \frac{\tau_m^0}{2}\left(\delta_m^f - \frac{(\delta_m^f - \delta_m^{\max})^2}{\delta_m^f - \delta_m^0}\right). \tag{12}$$

In Eq. (12) G_{max} is the area of the trapezoid expanding from origin to δ_m^{max} (Fig. 2). Assuming the load ratio as $R^2 = G_{min}/G_{max}$, ΔG can be written as:

$$\Delta G = \frac{\tau_m^0}{2}\left(\delta_m^f - \frac{(\delta_m^f - \delta_m^{\max})^2}{\delta_m^f - \delta_m^0}\right)(1 - R^2). \tag{13}$$

Finally, the final form of evolution of the damage parameter with subsequent cycles, Eq. (7), can be rewritten as:

$$\frac{\partial d}{\partial N} = \left\{ \begin{array}{cc} \frac{1}{A_{cz}} \frac{(\delta_m^f(1-d)+d\delta_m^0)^2}{\delta_m^f \delta_m^0} C\left(\frac{\frac{\tau_m^0}{2}\left(\delta_m^0 + \frac{(\delta_m^f - \delta_m^{\max})^2}{\delta_m^f - \delta_m^0}\right)(1-R^2)}{G_c}\right)^m & G_{th} < G_{max} < G_c \\ 0 & 0 \end{array} \right\}. \tag{14}$$

In Eqs. (10), (11a), (11b), (12)–(14), A_{cz}, stands for the cohesive zone area defined as the area from the crack tip to the point where the maximum cohesive traction is attained. Turon et al. (2007b) defined the A_{cz}, based on Rice's closed form equation (Rice, 1980). However, this equation was developed for pure Mode I loading and the model tends to be less accurate when subjected to mixed mode loading with higher mode II domination. In order to improve the functionality and accuracy of the model, in this work the estimation of the cohesive zone area is further improved for a mixed mode load case.

Cohesive zone length and consequently cohesive zone area is defined as a structural and material property. Different models have been proposed to estimate the length of the cohesive zone. The first estimation suggested by Dugdale (1960) is based on the size of the yield zone ahead of a mode I crack by idealizing the plastic region as a narrow strip extending ahead of the crack tip. In analogy to Dugdale (1960), Barenblatt (1962) provided a similar estimation for ideally brittle materials. Rice (1980) estimated the length of the cohesive zone as a function of the crack growth velocity. The expressions resulting from these models can be found in literature (Dugdale, 1960; Barenblatt, 1962 or Rice, 1980). Under plane stress conditions, for an isotropic material these models have a general form as:

$$A_{cz} = bE\frac{G_c}{\tau_0^2}. \tag{15}$$

Modified versions of Eq. (15) have been developed (Harper and Hallett, 2008) which for mode I and mode II components of the mixed mode loading can be written as:

$$A_{cz,I} = bE'\frac{G_{Ic}}{(\tau_n^0)^2}, \tag{16a}$$

$$A_{cz,II} = bE'\frac{G_{IIc}}{(\tau_s^0)^2}, \tag{16b}$$

E' is an equivalent elastic modulus for an orthotropic material, whose value depends on longitudinal and transverse modulus. For the transversely isotropic laminate here, the value of E' is assumed to be equal to the elastic modulus in thickness direction (E_{33}). b is the specimen width, $G_{IC}$and G_{IIC} are the critical energy release rate for mode I and mode II components of the mixed mode loading, and τ_n^0, τ_s^0 are the maximum interfacial strength of the cohesive element in normal and shear directions respectively.

Based on the detailed parametric studies conducted by Harper and Hallett (2008), the most reasonable mixed mode cohesive area

is predicted as the minimum possible area of the fully developed cohesive zone multiplied by a scaling factor M, using the formula:

$$A_{cz,mixed} = M[\min(\text{Equation 16a and 16b})]. \quad (17)$$

The applied scaling factor is chosen to be 0.5 by Harper and Hallett (2008) and 0.65 in this work, as it provides the best correlation between numerical and experimental results when compared to each other. $A_{cz,mixed}$, obtained through Eq. (17), is taken as the effective cohesive area in all the mentioned calculations of this work. The improvement achieved via reformulation of the cohesive zone area is shown schematically in Section 5.2 (Results and discussions).

It is worth mentioning that in all the different approaches considered for the evaluation of cyclic damage growth in literature (Maiti and Geubelle, 2005; Munoz et al., 2006; Nguyen et al., 2001; Peerlings et al., 2000; Roe and Siegmund, 2003; Serebrinsky and Ortiz, 2005; Turon et al., 2007b or Yang et al., 2001), as also in this work, either the degradation of the interface stiffness, K, or the evolution of the damage parameter, d, per cycle is defined explicitly.

3. Cyclic mixed mode bending (MMB) experimental procedure

3.1. Test specimens

The specimens tested here are 24-ply multidirectional carbon/PEEK laminates, 25 mm wide, 150 mm long, and 3.12 mm thick, manufactured by consolidation technique described in detail in (Naghipour et al., 2009a). The base material is APC2-prepreg consisting of AS4-carbon fibres (60 vol.%) impregnated with a PEEK matrix, and the thickness of each prepreg layer is about 140 μm. The stacking sequence and orientation of multidirectional layers (Table 1) are chosen according to two design criteria; minimizing the coupling stiffness, B_{ij}, and minimizing the non-dimensional flexural stiffness ratio, D_c in upper and lower sublaminates. In order to reduce the inevitable thermally induced residual contractions that occur during cooling after consolidation, coupling stiffness B_{ij} of the chosen laminates is desired to be zero or very close to zero (Daniel and Ishai, 1994 or Jones, 1975). The specimen stacking sequence is also chosen to minimize and keep the non-dimensional ratio of the specimens flexural rigidities, $D_c, (D_c = D_{12}^2/D_{11}D_{22})$ smaller than 0.25 in each delamination arm in order to minimize non-uniform toughness value distribution and the errors in the perceived values of critical fracture toughness (Davidson et al., 1995). To obtain a defined delamination according to the standard test method for mixed mode delamination (ASTM D6671, 2002) a 50 mm wide polyimide film (Kapton®) is placed in the mid-plane of each lay-up as a delamination starter. Accordingly, in layup 22.5 the delamination starter lies in between + 22.5°/−22.5° plies, and in layup QI it lies in between 90°/0° plies. All specimens were produced at the composite laboratory of the Institute of Structures and Design at German Aerospace Centre (DLR).

3.2. Experimental procedure and data reduction

The MMB experiment represented by a superposition of simple mode I and mode II loadings provides the possibility to combine the influence of normal (mode I) and shear stresses (mode II) on inter-laminar delamination using a single test apparatus. Fig. 4 shows the MMB loading expressed in terms of the applied load P, the loading lever length c, and the specimen half-span L. The test is now accepted as an international standard by ASTM for fibre reinforced composites (ASTM D6671, 2002). As there is not any standardized MMB test method under fatigue loading, a few specimens were tested to obtain the optimum test frequency and displacement amplitude for performing valid cyclic MMB experiments. Fatigue damage experiments of a MMB specimen with 50% mode ratio were then conducted to obtain the interfacial traction degradation and damage growth after applying successive loading cycles. Cyclic MMB experiments were conducted under displacement control. Based on the analysis suggested in (ASTM D6671, 2002), the loading lever length, c, was determined to be 65 mm for a mode mixity of 50%. In order to achieve reliable experimental results and minimize the data scatter, at least 5 specimens were tested for each layup with this mode mixity. MMB fatigue experiments were performed in a MTS servo-hydraulic test machine, with constant displacement amplitude. The chosen amplitude was equal to 55% of quasi-static displacement at failure and with a displacement ratio of 0 ($\delta_{min}/\delta_{max} = 0$). Although the numerical fatigue damage law considers the effects of different displacement ratios, only a displacement ratio of 0 is tested here for the case of simplicity. It is worth mentioning that quasi-static tests were conducted at German Aerospace Center and the detailed experimental procedure and results are summarized the previous paper of the authors (Naghipour et al., 2009b). In order to find an optimum frequency for the cyclic MMB experiment, 3 different test frequencies (1, 2, and 3 Hz) were examined. Taking the amplitude constant during the tests, the crack propagation with a frequency of 3 Hz was very fast and thereof the experimental data could not be recorded properly. In the conducted experiment with a frequency of 1 Hz the number of cycles to failure always exceeded 300,000 cycles, which was chosen as a maximum value for number of cycles to failure in our experiments. Therefore, test frequency was set to 2 Hz and the tests were performed at ambient temperature. The delamination crack growth was manually measured on both sides of the specimen with an instrumented traveling microscope. Crack tip positions were read at intervals, temporarily stopping the load cycling. Measurements were taken periodically until crack propagation rates reached below 10^{-8} mm/cycle or the test reached 300,000 cycles. Degradation of the measured load within successive cycles is recorded and compared with the load versus cycle degradation in the numerical simulation (Section. 5).

Table 1
MD CFRP specimen configurations.

Layups to be considered	Layup name	$\mathbf{D}_c$	Largest B_{ij}
$(+22.5/-22.5)_{12}$	Layup 22.5	0.229	0.0024
Quasi-isotropic ($[0/\pm 45/90]_6$)	Layup QI	0.076	0.0039

The data reduction procedure to calculate mode I and mode II strain energy release rates ($G_I$and G_{II}) for MMB specimen are derived from beam theory (BT) solutions (Williams, 1989). In order to obtain a general BT solution, the laminates here are assumed as general, non-homogenous multidirectional layups with asymmetric sub-laminates on the upper and lower portions of the delamination plane (Fig. 4). G_I and $G_{II}$are functions of applied load (P), loading lever length (c), propagating crack length (a), and mechanical and geometrical properties of the specimen. The BT equations are further corrected by energy associated with shear deformation, the rotation of arms at the delamination tip, and plastic deformation ahead of the crack tip incorporated as crack tip correction factors χ_n and χ_s. The corrected BT formulations are summarized in Eq. (18).

$$G_I = G_{DCB} = \frac{6P^2\left(\frac{\beta}{\alpha}+1\right)(a+\chi_n)^2}{\frac{\beta}{\alpha}E_{11f,u}b^2h_u^3}\left(\frac{(1+2\frac{\beta}{\alpha})c-L}{2(1+\frac{\beta}{\alpha})L}\right)^2 \quad \frac{\beta}{\alpha} = \frac{E_{11f,l}h_l^3}{E_{11f,u}h_u^3},$$
$$G_{II} = G_{ENF} = \frac{3P^2(a+\chi_s)^2}{2b^2E_{11f,u}h_u^3}\left(\frac{1}{\frac{\beta}{\alpha}+1}-\frac{1}{\eta}\right)\left(\frac{c+L}{L}\right)^2. \quad (18)$$

The crack tip corrections for normal and shear modes, χ_n and χ_s, are computed adapting the existing solutions for unidirectional com-

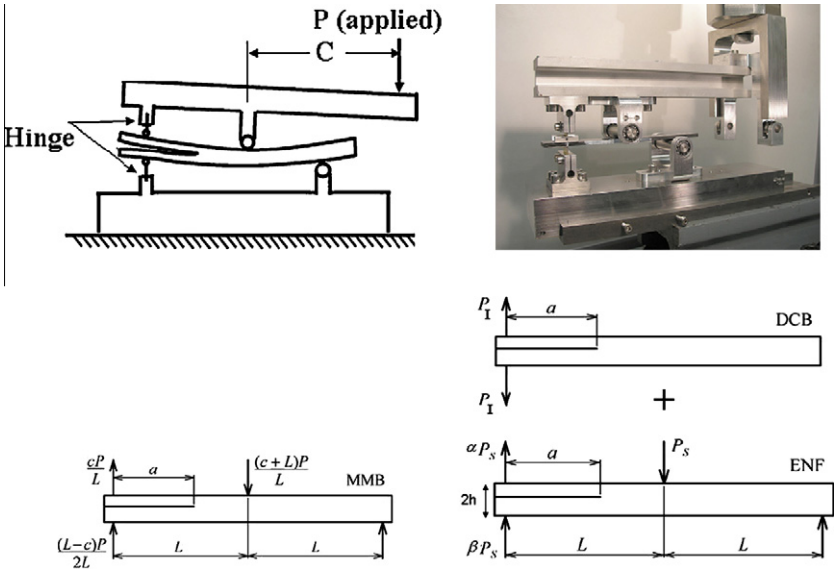

Fig. 4. Schematic and loading description of MMB test.

posites (Wang and Qioa, 2004; Williams, 1989) and are calculated as:

$$\chi_n = h_u\sqrt{\frac{E_{11f,u}}{11G_{13}}\left\{3-2(\Gamma/1+\Gamma)^2\right\}} \quad \Gamma = 1.18\frac{\sqrt{E_{11f,u}E_{22,u}}}{G_{13,u}},$$
$$\chi_s = h_u\sqrt{\frac{E_{11f,u}}{72G_{13,u}}}. \tag{19}$$

In order to calculate the critical strain energy release rates or fracture toughness, G_{IC} and G_{IIC}, applied load, P, and propagating crack length, a, values in Eq. (18) must be replaced by their critical values, P_c and a_c, respectively attained in the MMB experiment (Naghipour et al., 2009b). In the above expressions E_{11f} stands for longitudinal flexural modulus in fibre direction of the sublaminates obtained through Classical Laminate Theory. E_{22} and G_{13} are transverse modulus perpendicular to fibre direction and transverse shear modulus of the whole laminate, respectively. The subscripts (u) and (l) correspond to the upper and lower sublaminates, and b and h are width and half-thickness of the specimen. It is worth mentioning that the crack tip correction factors are assumed to be the same for upper and lower sublaminates here.

Using the cyclic MMB experiment outputs, Paris plot parameters (Fig. 5) can be extracted and further be used in the numerical cyclic damage model (Eq. (11b)). In the Paris equation, (Eq. (11a)), schematically shown in Fig. 5, G_{max} is the total strain energy release rate of the MD layups with 50% mode mixity. It is calculated using modified beam theory equations, within each loading cycle. Beam theory equations, used for calculation of G_{max} are given in Eq. (18). The growth rate da/dN (Fig. 5) is computed by calculating the slope of the line relating crack length (a) versus number of cycles (N), recorded throughout the experiment. Because of small delamination increments, this approximation is quite reasonable. The gradient and the intercept of straight line fits, give C and m, respectively. The threshold value of the strain energy release rate, G_{th}, is determined as the strain energy release rate, at which less than 1 mm delamination growth occurred during 300,000 cycles.

4. Numerical simulations; construction of the numerical model and characterization of input parameters

The numerical model is a combination of 24 individual plies with specified orientations (Table 1) together with interface

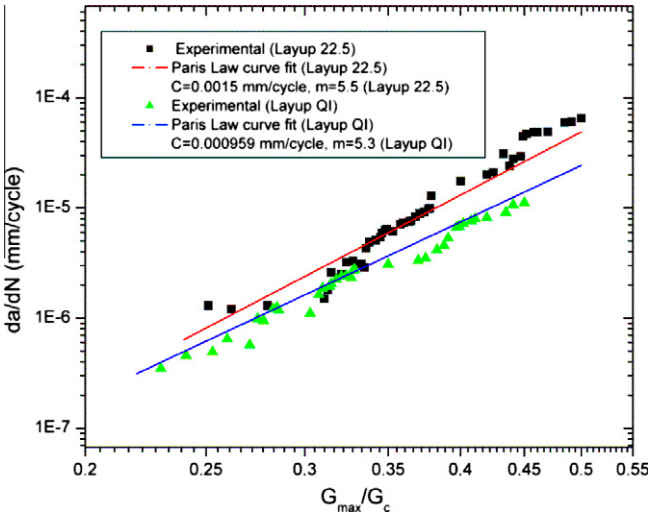

Fig. 5. Paris plot for a mode mixity of 50% showing experimental results and the linear regression.

elements, placed in the mid-plane of the laminate to capture the delamination behaviour. Each ply is assumed as an orthotropic continuum under plane stress modelled using reinforced ply model (Hashin, 1981) with 8 node, reduced integration shell elements. Interface elements are zero thickness, 8 node mixed mode cohesive elements, implemented as a user element in ABAQUS (2006) as described earlier in Section 2. Loading boundary conditions (displacements) are applied directly to middle and end supports (Fig.6).

The material properties required for the numerical cyclic MMB simulation are given in Table 2. For each lamina, X, Y, and S stand for ultimate in-plane strength in fiber, transverse, and shear directions with E_{11}, E_{22}, and G_{12}, representing the corresponding modulus, respectively. Mentioned laminar properties are determined from standard tension and compression coupon tests in fibre, matrix, and shear directions (Kohlgruber, 1997). For the interface element, $G_{Ic}$and G_{IIc}, are obtained using the Corrected Beam Theory data reduction scheme explained in Section 3.2. The parameter η is representing the mixed mode failure locus based on B–K failure criterion given in Eq. (5c). Normal and shear interfacial strengths are estimated to be 70–80 percent of resin strength and the math-

Table 2
Mechanical properties of lamina and interfaces of layup 22.5 and QI.

Mechanical properties of lamina (t: tension, c: compression) (Kohgruber, 1997)				
E_{11} (MPa)	E_{22} (MPa)	v_{12}	G_{12}(MPa)	G_{23} (MPa)
138,000	10,500	0.3	6300	3500
X_t (MPa)	X_c (MPa)	Y_t (MPa)	Y_c (MPa)	S (MPa)
2070	1360	86	196	147

Mechanical properties of interface (layup 22.5) Paris plot parameters: C = 0.0015 mm/cycle, m = 5.5, G_{th} = 0.08 mJ/mm^2					
τ_n^0 (MPa)	$\tau_s^0 = \tau_t^0$(MPa)	K (N/mm^3)	G_{Ic} (mJ/mm^2)	G_{IIc} (mJ/mm^2)	η
75	80	10^7	1.74	2.89	2.3

Mechanical properties of interface (layup QI) Paris plot parameters: C = 0.000959 mm/cycle, m = 5.3, G_{th}= 0.06 mJ/mm^2					
τ_n^0 (MPa)	$\tau_s^0 = \tau_t^0$ (MPa)	K (MPa)	G_{Ic} (mJ/mm^2)	G_{IIc} (mJ/mm^2)	η
75	80	10^7	1.36	2.21	2.25

ematical penalty value for the initial interfacial stiffness, K, is approximated to be 10^7 N/mm^3. The fatigue related Paris plot parameters are extracted from cyclic MMB experimental data (Fig. 5). Since the loading lever is not simulated, specified displacement increments are applied directly to middle and end supports, as shown in Fig. 6. The loading is defined in two steps: the first analysis loading step is quasi-static and it ends at the maximum applied displacement. It is assumed that no fatigue damage accumulation occurs during this step. Next, a second loading and unloading step is applied, in which the maximum displacement is held constant during the cycle, and the step time increment is assumed to be 0.1, so that 10 successive cycles can be simulated in a time step.

5. Results and discussion

5.1. Numerical simulation results and comparison to experiments

Having determined the required material parameters for the numerical model, degradation of the applied load within successive cycles predicted by the numerical simulation is compared with the load versus cycle degradation recorded during cyclic MMB experiments. The results obtained from the simulations and the experimental data are shown in Fig. 7a,7b. It can be observed that the constitutive model provides a successful prediction of the reduction of the applied load during successive cycles. For both layups the degradation starts with a moderate rate in the beginning of the second (cyclic) step, and slows down again within final cycles. Fig. 7a approves the significance of implementing the

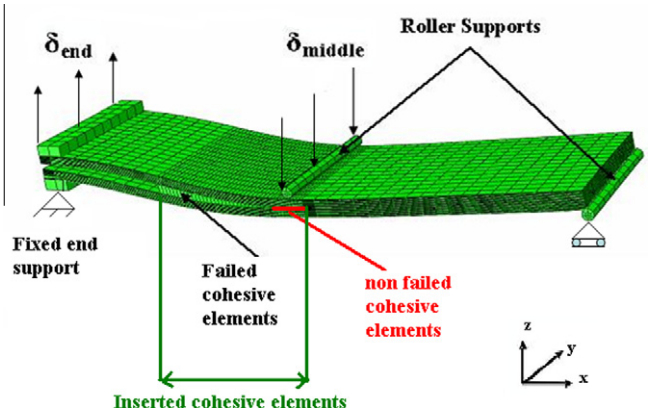

Fig. 6. Schematic view of the numerical model.

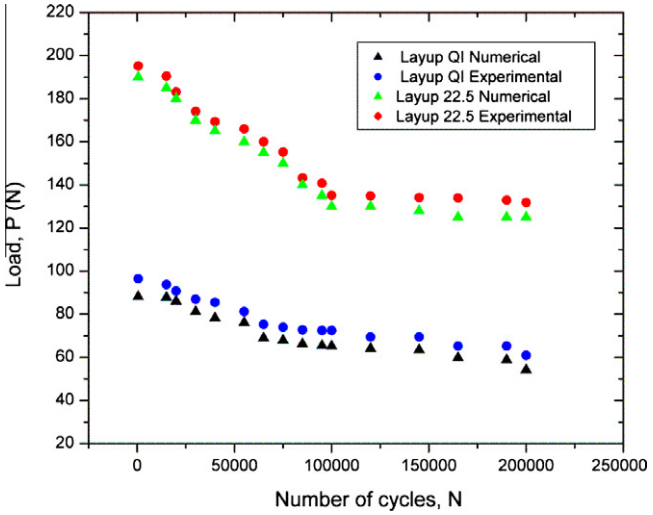

Fig. 7a. Reduction of the applied load (P) within successive cycles with addition of cyclic damage law to the constitutive law of the cohesive elements.

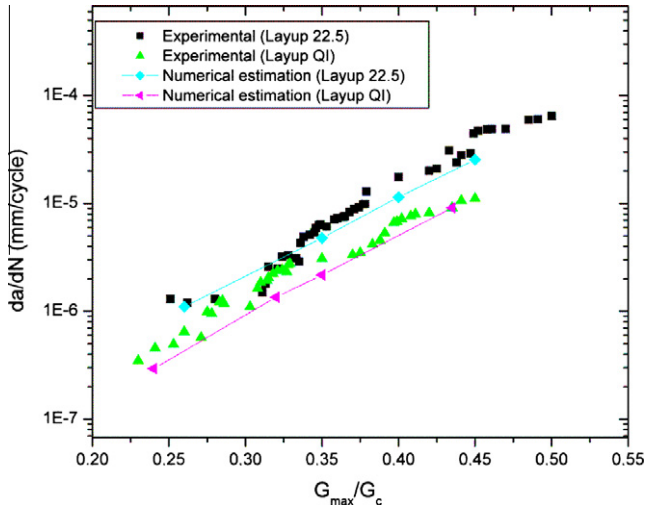

Fig. 7b. Comparison of experimentally and numerically obtained da/dN versus G_{max}curves.

cyclic damage law to the interface elements. Clearly without the addition of the fatigue damage variable, (d_{cyclic}), the real reduction of the applied force (P) can not be captured within successive cycles. Similar to the work of Munoz et al. (2006) the numerical model reproduces the Paris plot successfully compared to the experimentally obtained one. By adding the cyclic damage law, i.e. the cyclic damage parameter (d_{cyclic}), reduction of the applied load through successive cycles can be approximated with less than 10% error, which implies a reliable predictive capability of the numerical model under cyclic mixed mode loading. Redefinition of the cohesive area, according to Eq. (17), is one of the key factors improving the model's predicative capability under mixed modes, while some inaccuracy was reported in (Turon et al., 2007b) under mixed mode conditions. Crack propagation rate is faster in layup 22.5 compared to layup QI, which can also be observed in Paris plot (Fig. 7b). Numerically, this might result in higher growth rate of d_{cyclic} and higher degradation rate of the applied force (P) in layup 22.5, approved in Fig. 7a.

Damage initiation profiles depicted in the adjacent ply to the delamination plane, at the final specified displacement, are

compared for both layups (Fig. 8a, and 8b). In-ply matrix damage initiation criterion (Hashin, 1981) is nearly satisfied for layup QI, and the maximum value of damage initiation parameter reaches to 0.918, while in layup 22.5 it remains close to zero. This indicates the initiation of matrix ply damage in layup QI, which in turn leads to some amount of in-ply energy absorption and might be one of the reasons of the experimentally observed slower crack growth rate in this layup (Fig. 7b). Damaged matrix areas in layup QI are also observed during SEM observations, while no matrix damages were present in the SEM micrograph of layup 22.5 (Section 5.2). Possible interaction of in-ply and inter-laminar damage modes must always be taken into consideration in multidirectional laminates, in order to provide us with a reliable prediction of the ongoing fracture mechanism.

5.2. Effect of the cyclic increment, ΔN

In a degradation process involving high-cycle fatigue, a cycle-by-cycle analysis becomes computationally intractable. The cyclic increment is denoted by ΔN, and it must be determined properly in order to obtain solution convergence. For very small ΔN values the simulation will be rather accurate, because almost every single cycle would be simulated, however, the computational effort will be huge. On the other hand, when ΔN is too large, the predicted damage values for the next loading cycle, $N + \Delta N$, will be rather different from the exact solution of the differential equation. Similar to the approach presented by Munoz et al. (2006) in order to obtain proper and reliable values for ΔN, the load degradation curves with varying ΔN values are compared with the experimen-

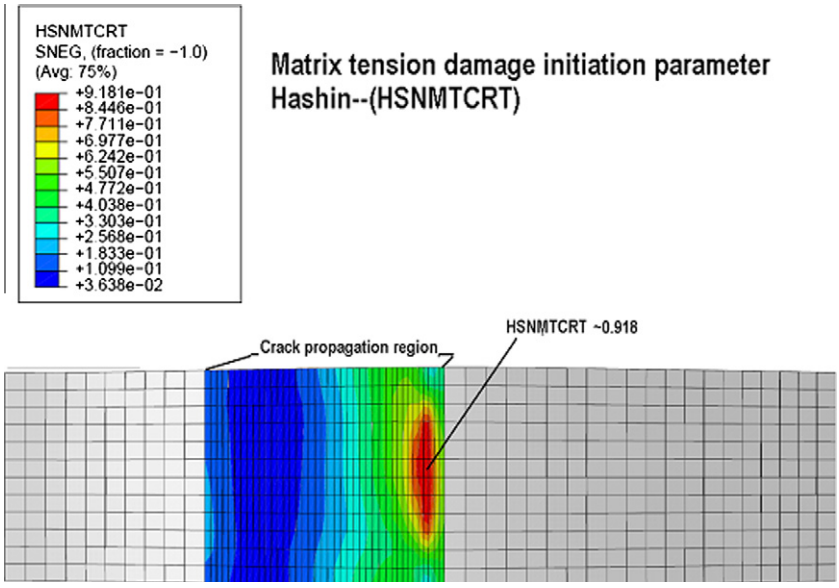

Fig. 8a. Damage initiation profile in the adjacent ply to the delamination plane in layup QI (HSNMTCRT: Hashin Matrix Tension Criterion).

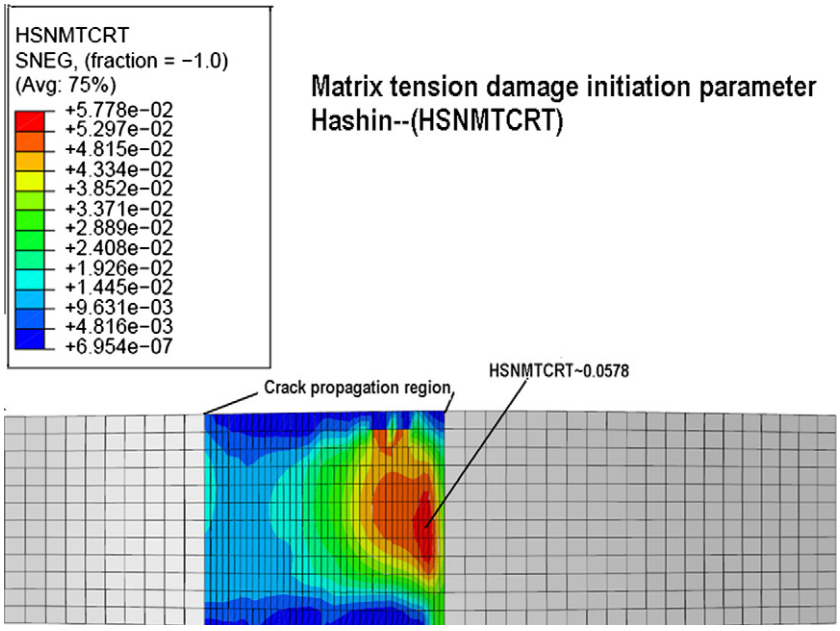

Fig. 8b. Damage initiation profile in the adjacent ply to the delamination plane in layup 22.5 (HSNMTCRT: Hashin Matrix Tension Criterion) matrix tension damage initiation parameter.

tally obtained result (Fig. 9). As long as a satisfactory convergence is achieved for the specified ΔN value, it can be assumed as an acceptable cyclic increment for the mentioned cyclic simulation. ΔN is chosen as 100, 200 or maximum 500 cycles in our numerical simulations (see Fig. 9).

5.3. Effect of the cohesive zone area, A_{cz}

Rice's closed form equation developed for pure Mode I loading (Rice, 1980) was used by Turon et al. (2007b) to define the cohesive zone area, A_{cz} in the cohesive element formulation. This might cause some inaccuracy when the model is subjected to mixed mode loading case with higher mode II ratios. Therefore, the estimation of A_{cz} in this work is further improved for a mixed mode load case utilizing the formulation of Harper and Hallett (2008) as described in Section 2.2. According to Harper and Hallett (2008) different approximations of A_{cz} can be achieved by varying the scaling factor, M, in Eq. (17) (Section 2.2). In Fig. 10 numerically obtained load degradation curves for various A_{cz} approximations are compared with the experimental result. It is observed that under a mixed mode loading case the A_{cz} obtained with the scaling factor of $M = 0.65$ provides a superior correlation with the experimental result compared to the A_{cz} suggested by Turon et al. (2007b). Hence, the scaling factor is taken as 0.65 in Eq. (17) and the respective $A_{cz,mixed}$ value is taken as the effective cohesive area in all the mentioned calculations of this work.

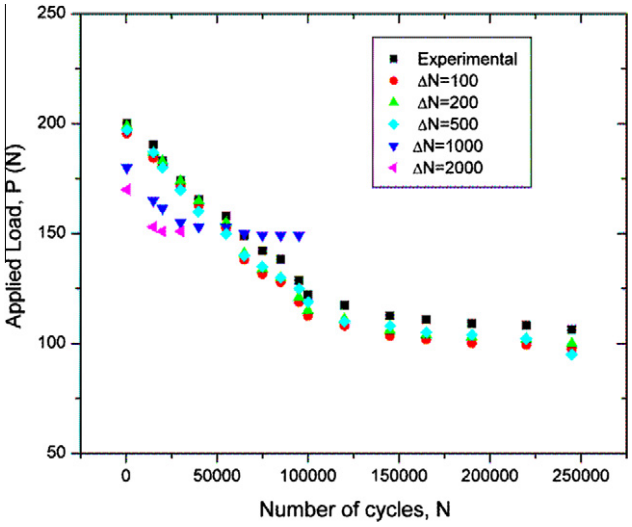

Fig. 9. Effect of ΔN value on numerical prediction of load reduction (Layup 22.5).

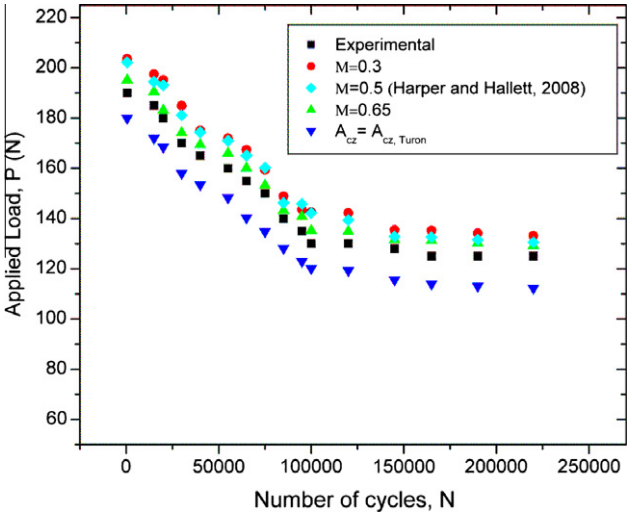

Fig. 10. Effect of A_{cz} estimation on numerical prediction of load reduction (Layup 22.5, mode mixity 50%).

5.4. Microstructure analysis of the failure surface under cyclic loading by SEM

Fracture surfaces of delamination cracks after cyclic loading in mixed mode bending under a mode mixity of 50% were investigated for layup 22.5 and layup QI by SEM, in order to obtain more detailed information about the ongoing cyclic damage mechanisms. The experimental conditions are mentioned in Section 3.2. Fig. 11 displays the fracture surface of layup 22.5 after 250,000 cycles, corresponding to the fully damaged cohesive zone in the specimen. It exhibits a relatively smooth surface when compared to the ones under quasi-static loading (Naghipour et al., 2009a,b). In similarity to the fracture surfaces under mixed mode quasi-static loading (Naghipour et al., 2009a,b), under cyclic loading a significant fracture feature is the appearance of asperities in the form of shear cusps, which are formed due to microcrack nucleation ahead of the crack tip and inelastic straining of the ligaments until rupture. The shear cusps after cyclic loading were more rounded than in quasi-static fracture surfaces and partially bent over the carbon fibres. Additionally some fine debris can be seen on the surfaces, which did not occur on fracture surfaces after quasi-static loading.

These features on the fracture surface after cyclic loading can be associated to the fact that the newly formed crack surfaces come in contact during the unloading part of the load cycles. Upon unloading and subsequent reloading the asperities rub against each other and this frictional interaction supposedly cause the abrasion of the asperities resulting in a smoother fracture surface under cyclic loading. This phenomenon of frictional fracture surface interaction is mainly responsible for the dissipation of energy in each unloading–reloading cycle. Thus, the cyclic failure can be interpreted as the result of interacting processes in front of the crack tip, i.e. the formation of microcracks in the resin and inelastic deformation of the ligaments forming shear cusps, and on the other hand processes behind the crack tip such as abrasion of the previously formed shear cusps during unloading. The abrasion of partially interlocking shear cusps, which act as crack bridging elements, reduces their load bearing capacity and increases the stress intensity at the crack tip. These processes microscopically result in a steady weakening and degradation of the interface and macroscopically in

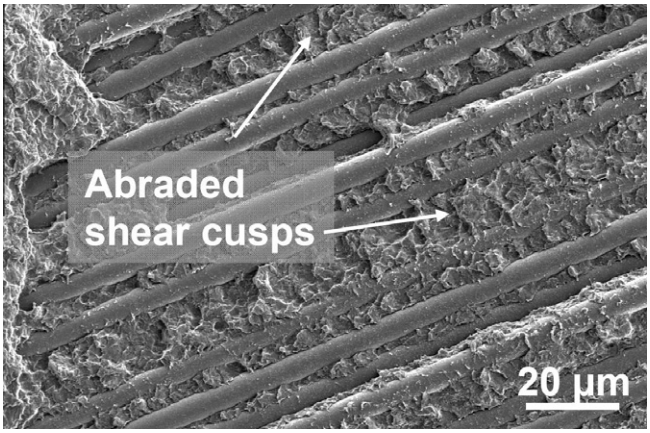

Fig. 11. Fracture surface with deformed and abraded shear cusps placed in between fibres (layup 22.5, 50% mode mixity, cyclic MMB) (crack propagation direction: from, left to right).

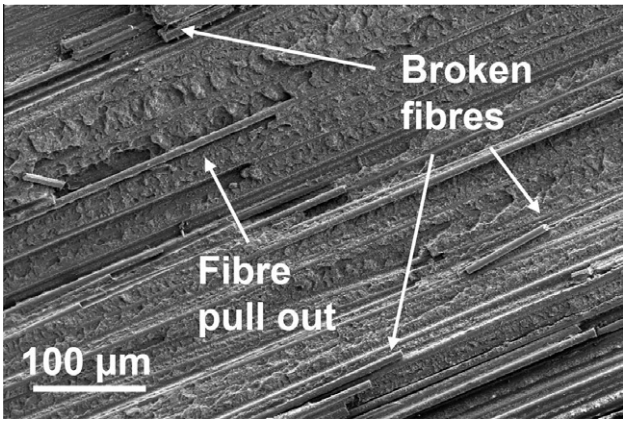

Fig. 12a. Broken fibres under cyclic mixed mode loading (layup 22.5, 50% mode mixity).

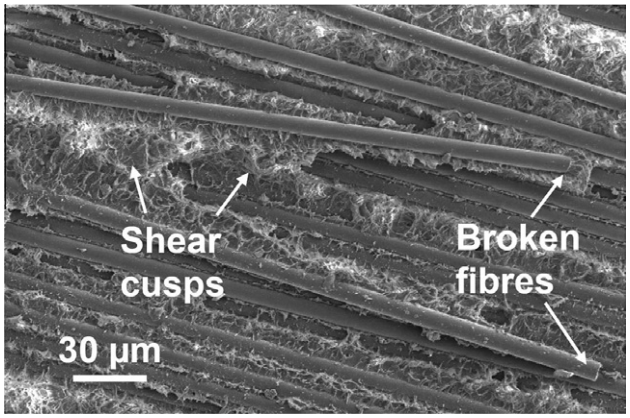

Fig. 12b. Fracture surface of layup 22.5 under quasi-static loading (50% mode mixity).

a reduction of the applied load in the dicplacement controlled MMB-fatigue test.

Appearance of broken fibres or fibres pulled out transversally to the longitudinal direction are important fracture surface characteristics observed both in cyclic (see Fig. 12a for layup 22.5) and quasi-static mixed mode loadings as shown in Fig. 12b (Naghipour et al., 2009b). The amount of broken fibres has been larger after fatigue than after quasi-static loading, which has been also reported by Russell and Street (1987). In some regions, the broken fibres appear chiefly in the form of fibre bundles (Fig. 13), which is a specific characteristic of cyclic loading as no broken fibre bundles were observed in mixed mode quasi-static fracture surfaces (Naghipour et al., 2009a,b). Broken fibres and fibres, which have been pulled out, have all adherent resin layers on them, which means that the fibre/matrix interface was very strong.

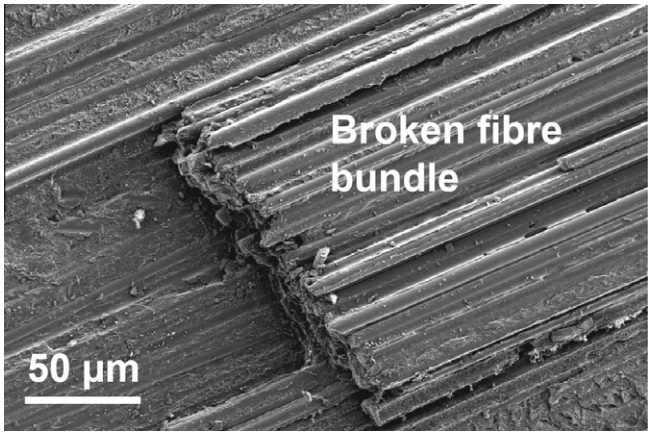

Fig. 13. Appearance of broken fibres in form of fibre bundle under cyclic mixed mode loading (layup 22.5).

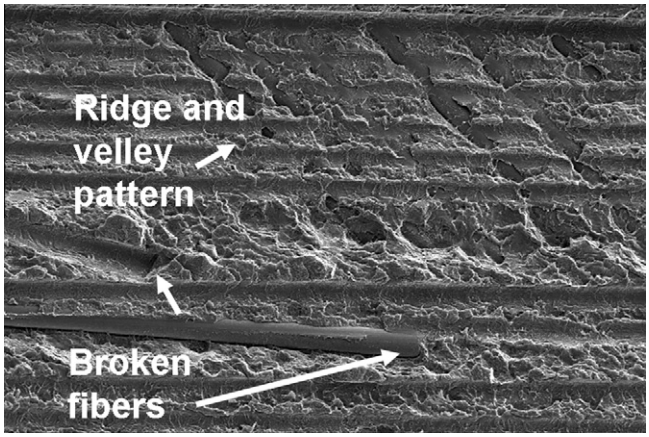

Fig. 14. Fracture surface with ridges and valleys in the fractured matrix (layup QI, 50% cyclic MMB).

Fig. 14 shows the fracture surface of layup QI after 280,000 cycles, exhibiting a relatively smooth surface with large amount of resin debris, which is also supposed to be a characteristic of fatigue failure (Marom, 1989). The fatigue failure of layup QI is dominated by matrix fracture. Matrix fracture areas, tilted slightly to the overall fracture surface, can be found in the related SEM micrograph (Fig. 14). Very few broken fibres are present in the fracture surface compared to layup 22.5. Ridge and valley markings observed in the micrograph are recognised as a characteristic of combination of peel and shear failures during matrix fracture (Hibbs and Bradley, 1987).

The exemplary fracture surfaces analyzed above belong to the mid-plane surface of lower sub-laminate. In all the specimens the delamination path was from left to right and the delamination stayed in the mid-plane of the laminate without deviating to lower or upper sub-laminates.

6. Conclusions

The cyclic mixed mode delamination failure in multidirectional composites has been investigated following experimental and numerical approaches. For both of the chosen multidirectional layups subjected to 50% cyclic mixed mode loading, the numerical model predicts the degradation of the applied load within successive cycles successfully when compared with the corresponding experiments. The numerical model is combined of individual plies and bilinear cohesive interface elements placed in the delamination plane. The constitutive behaviour of the interface elements has been further extended by adding a fatigue damage variable to establish the evolution of the damage variable within successive cycles in terms of the crack growth rate. Furthermore, redefinition of the cohesive zone area in the interface element formulation seems to provide a significant improvement on the accuracy of the model under mixed mode conditions, when compared to previous woks in literature. It is observed that only with implementing a cyclic damage variable in the cohesive interface element the experimentally observed crack growth and stiffness degradation can be captured properly. The numerical results also reveal

that in order to achieve a closer response to experimentally obtained results and to obtain solution convergence, the cyclic increment, ΔN, must not exceed a certain value. Finally, scanning electron microscopy was used for distinguishing the features of the fracture surfaces and to establish the differences between static and fatigue fracture, as well as the differences between the various modes of fracture in different multidirectional lay-ups. It appears that fracture surfaces after cyclic loading were much smoother than after quasi static loading due to repeated frictional interaction of the fracture surface during the unloading sequences. The fatigue failure of layup QI was dominated by matrix fracture and large amounts of resin debris was found in SEM micrographs. Nevertheless, the dominant failure mechanism in layup 22.5 was fibre fracture with high amounts of broken fibres and fibre bundles observed on the fracture surface. It is also concluded that in multidirectional laminates in-ply and inter-laminar damage modes might interact with each other and this must always be taken into consideration, in order to achieve reliable predictions of the ongoing fracture mechanism.

Acknowledgements

The authors acknowledge the effort of the technicians in the institute of Structure and Design of DLR in Stuttgart for producing the CFRP laminates and the experimental testing group, especially Janine Schneider and Dirk Lütz, for conducting the experiments and Liudmila Chernova for taking the SEM micrographs.

References

ABAQUS 6.6 User's Manuals, Hibbitt, Karlsson and Sorensen, 2006. Pawtucket. U.S.A.

Alfano, G., Crisfield, M.A., 2001. Finite element interface models for delamination analysis of laminated composites: mechanical and computational issues. Int. J. Numer. Methods Eng. 50, 1701–1736.

Allix, O., Blanchard, L., 2006. Mesomodeling of delamination: towards industrial applications. Compos. Sci. Technol. 66, 731–744.

Andersons, J., 1994. Methods of fatigue prediction for composite laminates; A review. Mech. Compos. Mater. 6, 545–554.

ASTM D6671-01, 2002. Interlaminar Standard Test Method for Mixed Mode I/ Mode II Fracture Toughness of Unidirectional Fiber Reinforced Polymer Matrix Composites. American Society for Testing and Materials (ASTM), PA, U.S.A.

Barenblatt, G.I., 1962. The mathematical theory of equilibrium cracks in brittle fracture. Adv. Appl. Mech. 7, 55–129.

Bathe, K.J, 2001. Finite Element Procedures. Springer, Berlin.

Benzeggagh, M.L., Kenane, M., 1996. Measurement of mixed-mode delamination fracture toughness of unidirectional glass/epoxy composites with mixed-mode bending apparatus. Compos. Sci Tech. 56, 439–449.

Blanco, N., Gamstedt, E.K., Asp, L.E., Costa, J., 2004. Int. J. Solids Struct. 4, 4219–4235.

Daniel, I.M., Ishai, O., 1994. Engineering Mechanics of Composite Materials. Oxford, New York.

Davidson, B.D., Kruger, R., Konig, M., 1995. Three dimensional analysis and resulting design recommendations for unidirectional and multidirectional end notched flexure tests. J. Compos. Mater. 29, 2108–2133.

Dowling, N., Begley, J., 1976. Fatigue crack growth during gross plasticity and the J-integral. ASTM STP 590, 82–103.

Dugdale, D.S., 1960. Yielding of steel sheets containing slits. Nonlinear Dyn. 8, 100–104.

Ewalds, H.L., 1984. Fracture Mechanics. Edward Arnold, London.

Harper, W.P., Hallett, S.R., 2008. Cohesive zone length in numerical simulations of composite delamination. Eng. Fract. Mech. 75, 4774–4792.

Hashin, Z., 1981. Failure criteria for unidirectional fiber composites. J. Appl. Mech. 20, 329–334.

Hibbs, M.F., Bradley, W.L., 1987. Correlations between micromechanical failure processes and the delamination toughness of graphite/epoxy systems. In: Masters, J.E., AU, J.J. (Eds.), Fractography of Modern Engineering Materials: Composites and Metals, vol. 948. American Society for Testing and Materials (ASTM) STP, Philadelphia, PA, pp. 68–97.

Jones, R.M., 1975. Mechanics of Composite Materials. McGraw-Hill, New York.

Kohlgruber, D. 1997. Internal report: Mechanical properties of PEEK/AS4. Source: CYTEC/DLR. Institute of Structures and Design, German Aerospace centre -DLR. Stuttgart.

Maiti, S., Geubelle, P., 2005. A cohesive model for fatigue failure of polymers. Eng. Fract Mech. 72, 691–708.

Marom, G., 1989. Environmental effects on fracture mechanical properties of polymer composites. In: Friedrich, K. (Ed.), Application of Fracture Mechanics to Composite Materials. Elsevier, Amsterdam, pp. 397–424.

McDowell, D., 1997. An engineering model for propagation of small cracks in fatigue. Eng. Fract Mech. 56, 357–377.

Munoz, J.J., Galvanetto, U., Robinson, P., 2006. On the numerical simulation of fatigue driven delamination with interface elements. Int. J. Fatigue 28, 1136–1146.

Naghipour, P., Schneider, J., Bartsch, M., Hausmann, J., Voggenreiter, H., 2009a. Fracture simulation of CFRP laminates in mixed mode bending. Eng. Fract. Mech. 76, 2821–2833.

Naghipour, P., Bartsch, M., Chernova, L., Hausmann, J., Voggenreiter, H., 2009b. Effect of fiber angle orientation and stacking sequence on mixed mode fracture toughness of carbon fiber reinforced plastics; numerical and experimental investigations. Mater Sci. Eng. A. 527, 509–517.

Nguyen, O., Repett, o E.A., Ortiz, M., Radovitzky, R.A., 2001. A cohesive model of fatigue crack growth. Int J Fract. 110, 351–369.

Paris, P., Erdogan, F., 1963. Critical analysis of propagation laws. J. Basic Eng. 85, 528–534.

Paris, P., Gomez, M., Anderson, W., 1961. A Rational analytical theory of fatigue. Trend Eng. 13, 9–14.

Peerlings, R.H.J., Brekelmans, W.A.M., de Borst, R., Geers, M.G.D., 2000. Gradient-enhanced damage modelling of high-cycle fatigue. Int. J. Numer. Methods Eng. 49, 1547–1569.

Reifsnider, K.L., 1991. Fatigue of Composite Materials. Elsevier.

Rice, J.R., 1980. The mechanics of earthquake rupture. In: Dziewonski, A.M., Boschhi, E. (Eds.), Physics of the Earth's interior, Proceedings of the international school of physics. Italian Physical Society/North-Holland, Amsterdam, pp. 555–649.

Roe, K., Siegmund, T., 2003. An irreversible cohesive zone model for interface fatigue crack growth simulation. Eng. Fract Mech. 70, 209–232.

Russell, A.J., Street, K.N., 1987. The effect of matrix toughness on delamination: static and fatigue fracture under mode II shear loading of graphite fibre composites, In: Johnston, N.J., (Ed.), Toughened Composites, American Society for Testing and Materials, (ASTM) STP, vol. 937, Philadelphia, pp. 275–294.

Serebrinsky, S., Ortiz, M., 2005. A hysteretic cohesive-law model of fatigue-crack nucleation. Scripta Materialia 53, 1193–1196.

Suresh, S., 1991. Fatigue of Materials. Cambridge University Press.

Szabó, B., Babuška, I., 1991. Finite element analysis. John Wiley and Sons Inc., New York.

Talreja, R., 1999. Damage mechanics and fatigue life assessment of composite materials. Int. J. Damage Mech. 8 (4), 339–354.

Turon, A., Dávila, C.G., Camanho, P.P., Costa, J., 2007a. An engineering solution for mesh size effects in the simulation of delamination using cohesive zone models. Eng. Fract. Mech. 74, 1665–1682.

Turon, A., Costa, J., Camanho, P.P., Davila, C.G., 2007b. Simulation of delamination in composites under high-cycle fatigue. Composites: Part A 38 (11), 2270–2278.

Wang, J., Qioa, P., 2004. Novel beam analysis of end notched flexure specimens for mode II fracture. Eng. Fract. Mech. 71, 219–231.

Williams, J.G., 1989. The fracture mechanics of delamination tests. J. Strain Anal. 24, 207–214.

Yang, B., Mall, S., Ravi-Chandar, K., 2001. A cohesive zone model for fatigue crack growth in quasi-brittle materials. Int. J. solids struct. 38, 3927–3944.